Real-Time Finite-Element Simulation of Linear Viscoelastic Tissue Behavior Based on Experimental Data

Mert Sedef, Evren Samur, Cagatay Basdogan

Realistic and Real-time Finite Element Simulation of Linear Viscoelastic Tissue Behavior Based on Experimental Data

Mert Sedef, Evren Samur, Cagatay Basdogan

College of Engineering, Koc University, Istanbul, 34450, Turkey

e-mail: lsedef@ku.edu.tr, esamur@ku.edu.tr, cbasdogan@ku.edu.tr

Abstract

The earlier research studies on real-time finite element modeling of soft tissue behavior for medical simulation and training applications have mainly focused on modeling and simulation of linear and nonlinear static (time-independent) tissue response. The real-time simulation of time-dependent viscoelastic behavior of soft tissues using finite element methods has been neglected due to the challenges in modeling and the high cost of computations. Moreover, most of the existing viscoelastic tissue models for simulating time-dependent effects are not realistic since they are not based on the measured material properties of live organ tissues. The lack of experimental data on viscoelastic material properties of live organ tissues has been a significant obstacle in the development of realistic models. This paper presents an end-to-end solution to real-time and realistic finite element simulation of viscoelastic tissue behavior based on the experimental data collected by a robotic indenter. First, we develop a viscoelastic finite element

model for soft organ tissues using linear tetrahedral finite elements. This model is derived from the generalized Maxwell solid. Then, the viscoelastic material properties of pig liver, measured by a robotic indenter, are integrated into the model for realistic visual and haptic simulation. Finally, a pre-computation approach based on the superposition principle and a multi-layered computational architecture are implemented for real-time rendering of nodal displacements and interaction forces.

Keywords: surgical simulation, haptic feedback, finite element modeling, viscoelasticity, soft tissue characterization, superposition, pre-computation.

1. Introduction

Virtual reality (VR) based surgical simulators that provide realistic visual and haptic feedback to its users is a promising technology for medical training [1]. The core component of a computer-based surgical simulation and training system is the development of realistic organ-force models. An organ-force model must display physics-based behavior while handling various types of boundary conditions and constraints. Developing real-time and realistic organ-force models is challenging not only due to non-linearity, rate, and time dependence in material properties of organs but also due to layered and non-homogeneous structure of organ tissues.

Both linear and non-linear finite element methods (FEM) have been used for developing real-time organ-force models [see the list of references in 1 and 2]. Achieving a computationally fast and stable simulation is possible using a linear static FEM model since the global stiffness matrix of the system is constant and can be inverted before the real-time simulation. However, the assumption of linearity is not valid for soft tissues having a complex non-linear behavior. A linear FEM model cannot simulate large organ deformations accurately. While non-linear FEM models display more realistic deformations than the linear ones, they have a greater computational complexity due to the non-constant stiffness matrix of the system.

FEM-based organ-force models can also be grouped as static and dynamic models based on whether inertial and viscous effects are taken into account or not. The static FEM models cannot simulate the time-dependent effects such as viscoelasticity. Due to the challenges in modeling and the high cost of real-time computations, only a few research groups have recently focused on the real-time simulation of viscoelastic tissue behavior. Debunne et al. [4] developed a robust, adaptive method for simulating dynamic deformations of a viscoelastic object in real-

time using an explicit finite element method. Instead of merging finite element equations in a large matrix system, explicit FEM solve each element independently through a local approximation, dramatically reducing the computational time. Hauth et al. [5] developed a viscoelastic finite element formulation for the visual simulation of viscoelastic deformable objects. They use a Maxwell solid with one memory parameter in their viscoelastic material model. To obtain a formulation for the shear relaxation function, they first assume a constant mechanical quality factor for the material and then find the parameters of the Prony series corresponding to the Maxwell model by matching their compliance functions while minimizing the relative error. They use mass lumping and nested tetrahedral meshes to reduce the number of real-time computations. Schoner et al. [6] introduced a method for simulating viscoelastic solids in real-time based on a parameter estimation method derived from physical measurements of real objects. To model the viscoelastic effects, they combine a DGFM (discrete Green's function matrix) with particle systems by replacing the spring-like relations in the DGFM with compositions of springs and dashpots. This provides the ability to simulate viscoelastic behavior while retaining the DGFM for the primary deformation calculations. Although they have achieved real-time update rates for visual display of deformations, they have chosen to use a quasi-static elastic model for calculating and reflecting interaction forces through a haptic device in real-time. Schwartz et. al. [7] developed a tensor–mass method for the finite element simulation of non-linear viscoelastic mechanical deformations in biological soft tissues. They introduce the material nonlinearity by locally modifying the stiffness tensors while keeping the strain tensor linear and adjusting the Lame constants. They use a Kelvin-Voigt viscoelastic element in their model and introduce a viscous force proportional to the deformation speed. The parameters of the simulation model are adjusted and validated by utilizing an experimental set-up

designed to characterize the material properties of biological tissues through in-vitro experiments.

We propose an end-to-end solution to real-time and realistic finite element modeling and simulation of viscoelastic soft tissue behavior. Our contributions include an efficient numerical scheme for the solution of a linear viscoelastic FEM model derived from the generalized Maxwell solid, methods for the measurement and integration of experimental data on viscoelastic material properties of soft tissues into the model for realistic display of visual deformations and interaction forces, and a pre-computation scheme and a multi-layer computational architecture for the real-time execution of the model with visual and haptic feedback to the user. The pre-computation approach has been suggested in the past for simulating linear FEM tissue models, but its extension to simulation of viscoelastic FEM models is by no means straightforward due to the rate and time-dependent effects.

In section 2, we provide a brief introduction to viscoelasticity and discuss the numerical solution of linear viscoelastic equations derived from the constitutive relation between stress and strain. We then introduce the formulations for a linear FEM model and then show its extension to modeling viscoelastic behavior. In section 3, we present methods for extracting viscoelastic material properties of soft tissues from the experimental data acquired by a robotic indenter. In section 4, we propose a pre-computation approach based on the superposition principle for the real-time rendering of forces and displacements and discuss the implementation details. In section 5, we validate our viscoelastic FEM model and the proposed pre-computation approach using ANSYS finite element package. Finally, the results and the possible future extensions of our work are discussed in section 6.

2. Linear viscoelasticity

2.1. Definition

A viscoelastic material is characterized by both elastic and viscous behavior. For elastic materials, Hooke's Law applies. Therefore, the stress is proportional to the strain, and the elastic modulus is defined as the ratio of stress to strain. On the other hand, the stress is proportional to the rate of the strain for a purely viscous material, and the ratio of stress to strain rate is known as viscosity. All the other materials that do not fall into one of these classifications are called viscoelastic materials. In viscoelastic materials, an instantaneous elastic response is observed upon loading, and then a slow and continuous change in the response at a decreasing rate is obtained. The rate of straining or stressing is an important factor affecting the time-dependent response of a viscoelastic material. For example, the longer the time to reach the final value of stress at a constant rate of stressing, the larger is the corresponding strain. For this reason, viscoelastic materials are said to keep a record of their response history and possess a "memory" [9]. This memory effect can be seen in the constitutive relationship between the stress and strain tensors.

One way of deriving a constitutive relationship for linear viscoelastic materials is to assume that a Boltzmann superposition of strain increments can be applied to viscoelastic materials. Consider an arbitrary strain input which is obtained through superposition of small strain increments

$$\varepsilon(t) = \sum_{j=1}^{n} \Delta\varepsilon_j = \int_0^t d[\varepsilon(s)] \tag{1}$$

where s is any arbitrary past time between 0 and t, when a constant strain ε is applied. The strain increments up to time t are related to corresponding stress increments by Hooke's law as follows

$$\sigma(t) = \sum_{j=1}^{n} \Delta\sigma_j(t - s_j) = \sum_{j=1}^{n} E(t - s_j)\Delta\varepsilon_j \tag{2}$$

Each of these stress increments also relax according to the time dependency of stress relaxation function E(t). By taking the appropriate limit, we get the following constitutive law

$$\sigma(t) = \int_0^t E(t - s)\frac{\partial\varepsilon(s)}{\partial s}ds \tag{3}$$

Viscoelastic materials are typically modeled by the generalized Maxwell solid [5, 9, 12] which is a combination of springs and dashpots. This type of model results in a Prony Series expression for the stress relaxation function in the form of

$$E(t) = E_\infty + \sum_{j=1}^{N} E_j e^{\left(\frac{-t}{\tau_j}\right)} \tag{4}$$

where N is the number of Maxwell elements, E_j's are the elastic coefficients (E_∞ is the long-term elastic modulus corresponding to the steady state elastic response of the system) and τ_j's are the relaxation times related to the damping coefficients of dashpots as η / E_∞.

2.2. Numerical computation of linear viscoelasticity

Splitting the integral in Equation 3 into elastic and viscoelastic contributions [9] leads to

$$\begin{aligned}\sigma(t) &= \int_0^t E_\infty \frac{\partial \varepsilon(s)}{\partial s} ds + \int_0^t \sum_{j=1}^{N} E_j \, e^{\left(-\frac{t-s}{\tau_j}\right)} \frac{\partial \varepsilon(s)}{\partial s} ds \\ &= E_\infty \varepsilon(t) + \sum_{j=1}^{N} \int_0^t E_j e^{\left(-\frac{t-s}{\tau_j}\right)} \frac{\partial \varepsilon(s)}{\partial s} ds \\ &= \sigma_0(t) + \sum_{j=1}^{N} h_j(t)\end{aligned} \tag{5}$$

By defining the step size as $\Delta t = t_{n+1} - t_n$, where t_{n+1} and t_n are the current and previous time steps, and substituting $\varepsilon(t) = \sigma_0(t)/E_\infty$ introduces a recursive formula for internal stress variables. The transition from differential coefficient to discrete time steps yields

$$h_j^{n+1} = e^{\left(-\frac{\Delta t}{\tau_j}\right)} h_j^n + \gamma_j \int_{t_n}^{t_{n+1}} e^{\left(-\frac{t_{n+1}-s}{\tau_j}\right)} ds \frac{\sigma_0^{n+1} - \sigma_0^n}{\Delta t} \tag{6}$$

where, $\gamma_j = \frac{E_j}{E_\infty}$ is the j^{th} normalized elastic modulus. If the above expression is integrated analytically, we obtain a recursive formula in 3D tensor representation given as

$$h_j^{n+1} = e^{\left(-\frac{\Delta t}{\tau_j}\right)} h_j^n + \gamma_j \frac{1 - e^{\left(-\frac{\Delta t}{\tau_j}\right)}}{\frac{\Delta t}{\tau_j}} \left[\sigma_0^{n+1} - \sigma_0^n\right] \tag{7}$$

Using the internal stress variables defined by the above equation and the elastic contribution, the total stress of a linear elastic Maxwell-material is defined as

$$\sigma^{n+1} = \sigma_0^{n+1} + \sum_{j=1}^{N} h_j^{n+1} \tag{8}$$

2.3. Linear static FEM formulation

A finite element representation of an organ can be constructed from 3-dimensional tetrahedral elements each having 4 nodes [8]. With known displacements within the element, U, the strains, ε, at any point can be determined by the following relation

$$\varepsilon = BU \tag{9}$$

where, B is a constant matrix defined by the shape functions. Assuming a linear elastic behavior, stress-strain relation is given by Hooke's law as

$$\sigma = C_{elastic}\ \varepsilon \tag{10}$$

where $C_{elastic}$ is a symmetric material stiffness matrix. Using the definition of internal force, we obtain

$$
\begin{aligned}
F_{int} &= \int B^T \sigma \, dV \\
&= \left(\int B^T C_{elastic} B \, dV \right) U \\
&= KU
\end{aligned}
\tag{11}
$$

where, $K = B^T C_{elastic} BV$ is defined as the element stiffness matrix and V is the volume of the element. Since internal and external forces balance each other within the element, $F_{int} = F_{ext}$, we end up with the well-known linear finite element equation given as

$$
KU = F_{ext} \tag{12}
$$

If the inverse of the stiffness matrix is calculated in advance, the static nodal displacements can be easily computed in real-time for the applied external forces ($U = K^{-1} F_{ext}$). The details of the linear FEM formulation utilizing tetrahedral elements for static tissue simulation are given in [8].

2.4. A numerical scheme for linear viscoelastic FEM formulation

To derive a similar expression for linear viscoelastic FEM formulation, we use the relations given in Equations 9 and 10 and the elastic contribution term

$$
\sigma_0^{n+1} = C_{elastic} \, \varepsilon^{n+1} \tag{13}
$$

Equation 8 can be written as

$$\begin{aligned}\sigma^{n+1} &= C_{elastic} B U^{n+1} + \sum_{j=1}^{N}\left[e^{\left(-\frac{\Delta t}{\tau_j}\right)} h_j^n + \gamma_j A_j \left(C_{elastic} B U^{n+1} - C_{elastic} B U^n \right) \right] \\ &= C_{elastic} B \left(1 + \sum_{j=1}^{N} \gamma_j A_j \right) U^{n+1} + \sum_{j=1}^{N} e^{\left(-\frac{\Delta t}{\tau_j}\right)} h_j^n - C_{elastic} B \left(\sum_{j=1}^{N} \gamma_j A_j \right) U^n \end{aligned} \tag{14}$$

where,

$$A_j = \frac{1 - e^{\left(-\frac{\Delta t}{\tau_j}\right)}}{\frac{\Delta t}{\tau_j}} \tag{15}$$

Using the definition given in Equation 11, an internal force expression is derived from Equation 14

$$F_{int}^{n+1} = K_T U^{n+1} + H^{n+1} - K_{hist} U^n \tag{16}$$

where, K_T is the constant tangent stiffness matrix, U^{n+1} and U^n are the vectors of nodal displacements at current and previous time steps respectively, K_{hist} is the history stiffness matrix, and $H^{n+1}$is the history matrix at current time step. If we consider the force balance at each time step,

$$F_{int}^{n+1} = F_{ext}^{n+1} \tag{17}$$

we end up with a general expression for linear viscoelasticity

$$K_T U^{n+1} = F_{ext}^{n+1} - F_{hist}^{n+1} \tag{18}$$

where internal load history vector of the object at current time step is

$$F_{hist}^{n+1} = H^{n+1} - K_{hist} U^n \tag{19}$$

Solving Equation 18 for U^{n+1}, we get an expression for the nodal displacements of a viscoelastic object under the influence of internal load history and the external load at current time step as

$$U^{n+1} = K_T^{-1}\left[F_{ext}^{n+1} - F_{hist}^{n+1}\right] \tag{20}$$

This expression is similar to the static finite element equation except the effect of time-dependent history term. Using Equations 12 and 15, the tangent stiffness matrix of each element, K_T is derived as follows

$$K_T = B^T C_{elastic} BV\left(1 + \sum_{j=1}^{N} \gamma_j A_j\right) \tag{21}$$

Turning back to Equation 20, F_{hist}^{n+1} is obtained via assembly of the element load history vectors at current time step

$$F_{hist}^{n+1} = H^{n+1} - K_{hist} U^{n} \tag{22}$$

H^{n+1} is the element history matrix at current time step, and represented as

$$H^{n+1} = V B^{T} \sum_{j=1}^{N} e^{\left(-\frac{\Delta t}{\tau_j}\right)} h_j^{\,n} \tag{23}$$

where $h_j^{\,n+1}$ for each element can be derived from Equations 7 and 13 as

$$h_j^{\,n+1} = e^{\left(-\frac{\Delta t}{\tau_j}\right)} h_j^{\,n} + \gamma_j A_j C_{elastic} B\left(U^{n+1} - U^{n}\right) \tag{24}$$

Going back to Equation 22, K_{hist} is the history stiffness matrix of each element and represented as

$$K_{hist} = B^{T} C_{elastic} B V \sum_{j=1}^{N} \gamma_j A_j \tag{25}$$

The numerical scheme for solving linear viscoelastic finite element equations is given in Figure 1. Given an external load, the pseudo code in Figure 1 solves for the nodal displacements.

********** **Figure 1** **********

3. Measurement and characterization of material properties of soft tissues

One of the main obstacles in the development of realistic organ-force models is the lack of data on material properties of live organ tissues. Measurement and characterization of in-vivo organ properties in a living body is a highly challenging task, but a requirement for realistic organ-force modeling. Organ-force models with incorrect material properties will result in adverse training effects in VR-based surgical simulator systems.

The research on tissue mechanics is extensive, but most of the earlier experiments have been performed in a laboratory environment (in-vitro studies) under well-defined boundary and loading conditions. Typically, tissue samples taken from an organ of interest are transferred to a laboratory in a chemical solution for measurements. Since the sample geometry and the experimental conditions are carefully decided in advance, stress and strain values are easily obtained from the measurement data. However, it is known that mechanical properties of soft tissues change with time and the results obtained through in-vitro measurements do not actually represent actual tissue properties.

We developed a robotic indenter for minimally invasive measurement of live tissue properties in a living body [3]. The system includes a robotic arm (Phantom Haptic Device, Model 1.0 from Sensable Tech. Inc.), a force sensor (Nano 17 from ATI Industrial Automation Inc.) and a long probe with a round tip of radius of 2 mm (Figure 2a). The force sensor is attached to the proximal end of the probe which is designed to be inserted through a surgical trocar (i.e. a port for inserting the surgical instruments to access the internal organs during a minimally invasive surgery). A PID controller was developed to command the robotic arm such that the probe tip followed the given path in 3D space with a desired velocity during the

experiments. A graphical user interface (GUI) was developed to record current time, displacement and force data in a text file following each experiment. Using the robotic indenter, we conducted stress relaxation experiments with 3 pigs and successfully measured the viscoelastic material properties of pig liver under 4 different loading conditions. The liver of each pig was indented to the depths of 2, 4, 6, and 8 mms in one second and the indenter was held there for 30 seconds to record the force response of liver as a function of time (i.e. force relaxation function, F(t)). The viscoelastic material properties of pig liver was then estimated from the stress relaxation function. The stress relaxation function defined by the generalized Maxwell solid results in a Prony series representation given in Equation 4. The coefficients of the Prony series for N = 2 (i.e. viscoelastic material properties: $E_\infty, E_1, E_2, \tau_1, \tau_2$) were determined via curve fitting to the experimental relaxation data (Figure 2b). For this purpose, we first obtained the shear relaxation function, G(t), from the experimental force relaxation function, F(t), using the small deformation assumption [11] ($G(t) = 3F(t)/16\delta\sqrt{R\delta}$, where δ is the indentation depth and R is radius of the indenter tip) and then obtained the stress relaxation function using the relation $E(t) = 2G(t)(1+\nu)$, where, ν is the Poisson's ratio and equal to 0.5 for soft tissue (Figure 2b). Finally, the normalized values of elastic moduli, $\gamma_j = E_j/E_\infty$, used in our numerical computations (see Figure 1) are obtained from the averaged values of short-term (E_1 and E_2) and long-term moduli (E_∞) of 3 pigs. The results of the stress relaxation experiments suggest that pig liver exhibit almost linear viscoelastic response. As shown in Figure 2c, the experimental stress relaxation data for different loading rates overlap each other.

********** **Figure 2** **********

4. Real-time simulation using pre-recorded displacement and force response

4.1. Simulation environment

We simulate real-time behavior of a 3-dimensional linear viscoelastic organ model with visual and haptic feedback to a user. The hardware components of our simulation system include a computer monitor to display visual interactions between the model and a virtual pointer, and a haptic device (PHANToM Model 1.0 A from SensAble Technologies) for simulating force interactions (Figure 3a). While a 3-dimensional volumetric model (made of tetrahedral elements) of human liver is used in our finite element computations, a triangular surface representation constructed from the surface nodes of the volumetric model is used in our graphical simulations. The underlying code is written in MS Visual C++ environment, the graphical rendering of the object and the visual deformations are displayed using Open Inventor (a scene graph API), and the haptic feedback to the user is provided via PHANToM haptic device using GHOST v.4.0 driver (Figure 3b).

********** Figure 3 **********

4.2. Haptic rendering

It is known that haptic rendering loop is much more demanding than the graphical rendering loop in displaying 3D objects. For rendering rigid objects, the interaction forces between a haptic probe and a 3D object must be updated at 1 kHz. For rendering deformable objects, this rate is lower, but still leaves a very short time for executing the underlying physics-based model to calculate the nodal displacements and interaction forces. In haptic rendering of

static FEM deformations, the nodal displacements can be calculated in real-time using the FEM equation ($U = K^{-1}F$) assuming that the inverse of the stiffness matrix is stored in advance. However, in rendering viscoelastic deformations, one must consider the effect of loading history in displacement computations (see Equation 20). This small change in the FEM formulation results in a significant increase in the number of computations. In fact, the direct implementation of the pseudo-code given in Figure 1 is computationally too expensive to execute in real-time and not suitable for haptic simulation. In particular, the number of computations in Section C is a major bottleneck. For example, the pseudo-code given in Figure 1 executes the computation of nodal displacements of a 3D cube consisting of $N_v = 51$ vertices, $N_{dof} = 153$ degrees of freedom, and $N_e = 136$ tetrahedrons in approximately 1.8 seconds on a Pentium IV 2.4GHz dual-processor personal computer for an external force applied to the nodes on the top surface of cube for 1 seconds ($\Delta t = 1$ msec). For a relatively finer model, consisting of $N_v = 380$ vertices, $N_{dof} = 1140$ degrees of freedom, and $N_e = 1659$ tetrahedrons, the same computation takes 40 seconds. In particular, there is a complex multiplication of a N_{dof} x N_{dof} full matrix with a N_{dof} x 1 full vector in Section C.III, and that complexity is directly proportional to the number of vertices in the mesh. Overall, the number of computations is $O(N^2_{dof})$.

4.3. Implementation details

In order to calculate the nodal displacements and interaction forces in real-time, we take advantage of the linearity and the superposition principle. Before the real-time simulation, we record the displacement and force response of each surface node and its neighboring nodes to a unit step force and a unit step displacement respectively. During the real-time simulation, we use the pre-recorded responses of the contacted node and its neighboring nodes to calculate the

resultant nodal displacements and interaction forces. While the pre-computation has been suggested and implemented for real-time simulation of static FEM in the past, the extension of this approach to a viscoelastic FEM simulation is not straightforward since the displacement and force response of nodes are rate and time-dependent. However, this rate and time-dependent behavior is important for displaying the true viscoelastic nature of the object. In our real-time simulations, for example, the user feels the force relaxation response of a viscoelastic model when the haptic probe penetrates into it and is held there for a while. The user can also visually observe the slowly changing recovery displacements of the nodes when the probe is removed. To reduce the number of computations, we assume that the recovery response of the nodes lasts for 30 seconds (In our animal experiments, we observed that the force relaxation response of pig liver for different loading rates lasts for approximately 30 seconds, see Figure 2c). In addition, only the nodes around the contacted node within a finite *Radius of Influence* (ROI) are assumed to be influenced by the loading. To calculate the displacement of a node at any time instant, the effect of all the past penetrations occurred up to that instant are superimposed. This requires to keep track of all previous contact events with their time of occurrence and simultaneously access the pre-recorded data of previously contacted nodes and their neighbors. This is a highly challenging task to accomplish in a single cycle of haptic loop. For this reason, at this stage, the displacement response of each surface node is calculated based on the superposition principle at a rate of 100Hz while the haptic loop is updated at 1 kHz. Between two consecutive cycles of the displacement calculations (Δt = 10 msec), we feed the haptic device with the pre-recorded force response of the contacted node for 10 msec.

4.3.1. Pre-recording phase. We first determine the neighbors of each surface node within a ROI. We then record two sets of data for each surface node of the model. The first set stores the force response of each surface node of the model and the displacement response of its neighboring nodes to a unit step displacement applied to it for 30 seconds. The second set stores the recovery displacement response of each surface node and its neighboring nodes for 30 seconds when a unit step force is applied to it for 10 msec (recall that the pre-recorded displacements are superimposed at 100 Hz). During the real-time interactions, if there is a collision, we use both data sets to calculate the nodal displacements and reaction forces. If there is no collision, we use the second data set only to calculate and display the nodal relaxations.

To construct the first data set, we conduct *virtual* stress-relaxation experiments with the viscoelastic FEM model. In a typical stress-relaxation experiment conducted with an actual tissue sample, a step displacement is applied to the sample and the relaxation of force is recorded until a steady state force value is reached. Since the only input to our viscoelastic FEM model is force and the nodal displacements are returned as output (Equation 20), we perform a reverse operation to obtain the force relaxation response of each node to a unit step displacement. We individually apply the Prony series representation of the experimental force relaxation data to each surface node of the viscoelastic FEM model to calculate the corresponding step displacement profile at the applied node and its neighboring nodes. We then scale the force-relaxation curve at the applied node such that its nodal displacement is exactly 1 mm (Figure 4a). The first 10 msec of the scaled force data is recorded as the *force-response* of the applied node and the constant-valued nodal displacements of its neighbors (less than 1 mm) are recorded as the *displacement-response* of the applied node.

To construct the second data set, we conduct *virtual* creep experiments with the viscoelastic FEM model. We apply a unit step force to each surface node of the model for 10 msec and record the corresponding displacement response of the applied node and its neighboring nodes for 30 seconds as the *recovery-displacement-response* of the applied node (Figure 4b).

********** Figure 4 **********

4.3.2. Real-time computation phase. Our real-time computational architecture for simulating linear viscoelasticity consists of three threads running asynchronously: *Haptic Thread, Force-Displacement Thread*, and *Visual Thread* (Figure 5). The *Haptic Thread*, updated at 1 kHz, acquires the new position of the haptic probe as the user manipulates the probe. If a collision is detected, the *Haptic Thread* reflects the calculated interaction forces back to the user through the haptic device. The *Force-Displacement Thread*, updated at 100 Hz, performs collision detection and calculates the collision response based on the superposition principle. Finally, the *Visual Thread*, updated at 30 Hz, graphically renders the haptic interface point (HIP) and the deformations of the model.

********** Figure 5 **********

At each cycle of the *Force-Displacement Thread*, we first determine the current (deformed) state of the object. For that purpose, displacement of a node at the current time step is calculated by first scaling the *recovery-displacement-responses* of each penetration occurred in the past with the magnitude of reaction force calculated for that penetration and then

superimposing the scaled displacement responses. Since we assume that *recovery-displacement-response* of a node converges to a constant value after 30 secs and the *Force-Displacement Thread* is updated at 100Hz, the maximum number of superposition operations due to the past penetrations can be at most 3000.

We then check the collisions between the current position of HIP and the current state of the object. If HIP is outside the object, no force is displayed to the user and the superimposed nodal displacements are sent to the *Visual Thread* for graphical rendering. If there is a collision, the penetration vector is calculated as the difference between the current positions of HIP and the *contact-node* (Our geometric database returns the nearest surface node of the undeformed model to the HIP as the *contact-node*). The reaction force for the next 10 msec is calculated by scaling the *force-response* of the *contact-node* by the penetration vector. This force profile is then sent to the *Haptic Thread* to be displayed to the user through the haptic device until the next cycle of the *Force-Displacement Thread*. To determine the nodal displacements due to the effect of current penetration only, the position of the *contact-node* is set to the current position of HIP and the *displacement-response* of the *contact-node* is scaled by the magnitude of penetration vector. To calculate the final displacements of neighboring nodes, their displacements due to the current penetration are added to their displacements due to the past penetrations (Figure 6). In addition, the information about the current penetration (i.e. *contact-node*, time of occurrence, reaction force) is added to the database of past penetrations to be used for future calculations in upcoming cycles. Finally, the nodal displacements are sent to the *Visual Thread* for graphical rendering.

********** **Figure 6** **********

Time complexity of our real-time computation phase is mainly governed by the nodal displacement calculations. Since the *recovery-displacement-response* of all penetrations occurred up to the current time step are superimposed, the complexity is *O(number of penetrations x number of neighboring nodes of each penetration)*, where the number of neighbors of a node grows quadratically as the underlying mesh becomes finer.

5. Validation

To validate our viscoelastic FEM model and the proposed pre-computation approach, we conducted simulation experiments with a 3D cube consisting of N_v = 51 vertices, N_{dof} = 153 degrees of freedom, and N_e = 136 tetrahedrons. The nodes at the bottom surface of the cube are constrained to have zero displacements in the vertical y-direction. In order to validate our linear viscoelastic FEM, we performed three different compression tests with the 3D cube. We then repeated the same compression tests using ANSYS finite element package and compared the results (Figure 7). In the first test, we applied 2.0 N to the center node on the top surface of the cube. The displacement response calculated using our viscoelastic FEM model and the one calculated using ANSYS show a perfect agreement up to the second digit after the decimal point (Figure 7a). In the second test, we applied 1.0 N to all nodes on the top surface for 30 seconds. The resultant displacement responses of our viscoelastic FEM and the ANSYS model are shown in Figure 7b. In the third test, we applied 1 mm displacement to all nodes on the top surface for 30 seconds using ANSYS to obtain their force relaxation response. Then, this response is applied to the same nodes of our viscoelastic FEM model to reconstruct their unit step displacement profiles (Figure 7c). The results of all compression tests conducted with our viscoelastic model perfectly match with that of ANSYS.

********** **Figure 7** **********

After demonstrating that our viscoelastic model works accurately, a real-time test with the haptic device was performed to validate the proposed pre-computation approach (Figure 8). First, the center node on the top surface of cube was indented to a certain depth using the haptic device and was held there for a while. Then, it was released and one of the neighboring nodes was indented. The nodal displacements and the force response of all the nodes on the top surface were recorded (Figure 8a and 8b). In order to compare our pre-computation approach with the direct solution of linear viscoelastic FEM model, the reaction forces recorded during the real-time interactions were supplied to our viscoelastic FEM model as an input to obtain the nodal displacements (Figure 8c). As it is shown in Figure 8d, the maximum error between the displacement values calculated through superposition approach and ones calculated through the direct solution of linear viscoelastic FEM model is less than one hundreds of a millimeter for nodal displacements of a few millimeters.

********** **Figure 8** **********

6. Discussion

There are only limited number of studies on real-time viscoelastic simulation of tissue behavior using finite elements for medical training applications. This is difficult because the displacement response of viscoelastic objects is time-dependent and influenced by the rate of loading. In addition, most of the existing viscoelastic soft tissue models are not realistic since

they are not based on the measured material properties. This study aims to close the gap between the real-time simulation and realistic simulation of soft tissue behavior. In this paper, we presented an end-to-end solution to the real-time and realistic simulation of viscoelastic soft tissue behavior based on the experimental data acquired by a robotic indenter. The development of finite element formulations to simulate viscoelastic tissue behavior is by no means straightforward. We developed a linear viscoelastic finite element formulation derived from the generalized Maxwell model with N elements. We put the final viscoelastic FEM equation (Equation 20) in a form similar to the well-known static equation (Equation 12) to clearly show the effect of time-dependent terms. This formulation enables the integration of viscoelastic material properties obtained from the stress relaxation experiments into to the model for realistic simulation of tissue behavior. Since the integration of incorrect material properties into organ-force models for simulating surgical procedures may result in adverse training effects, acquisition and characterization of material properties of soft tissue in a living body is an important and necessary step towards the development of realistic surgical simulators. Most of the existing organ-force models are optimized for real-time rendering and are not based on measurement data for realistic rendering. The lack of experimental data on viscoelastic material properties of live organ tissues has been a significant impediment in the development of realistic organ-force models. Most tissue characterization experiments conducted in the past have been performed in a laboratory environment outside the living body (in-vitro), but the recent studies show that the material properties obtained through in-vitro studies are different than the ones obtained through in-vivo studies. Our robotic measurement system is specifically designed to collect data from live organ tissues and it does not require any changes in the surgical procedures used for a minimally invasive surgery. Using this system, we conducted stress relaxation

experiments with 3 pigs to characterize the viscoelastic material properties of pig liver [3]. The viscoelastic material coefficients of pig liver were determined via curve fitting to the experimental stress-relaxation data. The long-term elastic modulus obtained through this process (E_∞ = 12.879 ± 2.95 kPa) corresponds to the effective linear elastic modulus of pig liver and show a good agreement with the values obtained by Ottensmeyer [10]. However, we should emphasize that there is a significant variation in the material properties of pig liver reported in the literature [3]. One possible cause of this variation is the difference between the measurement devices (e.g. hand-held probes versus robotics-based approaches) and the techniques (e.g. in-vitro versus in-vivo). The material properties of soft tissues obtained through in-vivo measurements are obviously closer to the actual properties, but the results should still be interpreted with caution since tissue response is location and direction dependent. In addition, the small indentation assumption used in our analysis affect the computation of viscoelastic material coefficients. Gefen and Marguilis argue that the small indentation assumption is valid up to 4 mm indentations made by a 2 mm radius round probe [11]. For this reason, we used the stress relaxation data of 4 mm indentations in our analysis and simulations. However, we observed that pig liver shows linear viscoelastic response (Figure 2c) and hence, the stress relaxation function corresponding to any other penetration depth could also have been used in our analysis and simulations.

We also implemented a pre-computation approach based on the superposition principle for the real-time simulation of the viscoelastic FEM model. The direct implementation of the pseudo-code given in Figure 1 is not feasible for the real-time haptic simulation since the number of computations is $O(N^2_{dof})$. However, the complexity of the suggested pre-computation approach is proportional to the number of past penetrations times the number of neighboring

nodes around the contact node of each penetration. The pre-computation approach has been applied to real-time static FEM simulation in the past, but, to our knowledge, it has not been extended to the real-time linear viscoelastic FEM simulation. The major difference from the static case is the inclusion of time and rate dependent effects which requires us to consider loading history of nodes in our displacement computations at each cycle of the simulation. For the implementation, we recorded the force and displacement responses of surface nodes of the viscoelastic FEM model to a unit step displacement and force respectively before the real-time simulation, and then use the pre-recorded data during the real-time simulation for the computation of time-dependent nodal displacements and forces. The developed model and the proposed pre-computation approach have been both validated using ANSYS finite element package. In the current implementation, we pre-calculate and record the *displacement-response, force-response,* and the *recovery-displacement-response* of each surface node in the form of individual data points. This consumes significant storage space in memory. In the future, we plan to employ curve fitting methods to store the pre-recorded data as a set of coefficients rather than individual data points.

References

1. Basdogan, C., De, S., Kim, J., Muniyandi, M., Srinivasan, M.A., (2004). “Haptics in Minimally Invasive Surgical Simulation and Training”, IEEE Computer Graphics and Applications, Vol. 24, No.2, pp. 56-64.

2. Basdogan, C., Ho, C, and Srinivasan, M. A., (2001). “Virtual environments for medical training: Graphical and haptic simulation of common bile duct exploration,” IEEE/ASME Transactions on Mechatronics, Vol. 6, No. 3, pp. 267-285.

3. Samur, E., Sedef, M., Basdogan, C., Avtan, L., Duzgun, O., (2005). “A Robotic Indenter for Minimally Invasive Characterization of Soft Tissues. Proceedings of the 19th International Conference on Computer Assisted Radiology and Surgery”, Vol. 1281 , pp. 713-718 , June, Berlin.

4. Debunne, G., Desbrun, M., Cani, M.P., Barr, A.H., (2001). “Dynamic real-time deformations using space & time adaptive sampling”, Proceedings of SIGGRAPH, ACM Press, pp. 31.36.

5. Hauth, M., GroB, J., StraBer, W., (2003). “Interactive Physically Based Solid Dynamics”, Eurographics/SIGGRAPH Symposium on Computer Animation.

6. Schoner J.L., Lang J, Seidel H.-P., (2004). “Measurement-Based Interactive Simulation of Viscoelastic Solids”, Proceedings of the Eurographics 2004, Vol. 23, No. 3.

7. Schwartz J.-M., Denninger M., Rancourt D., Moisan C., Laurendeau D., (2005). “Modeling liver tissue properties using a non-linear visco-elastic model for surgery simulation”, Medical Image Analysis 9(2), pp. 103-112.

8. Bro-Nielsen, M., Cotin, S., (1996). “Real-time volumetric deformable models for surgery simulation using finite elements and condensation”, Computer Graphics Forum, 15(3):57-66 (Eurographics'96).

9. Kaliske, M., Rothert, H., (1997). “Formulation and implementation of three-dimensional viscoelasticity at small and finite strains”, Computational Mechanics, Vol. 19, pp. 228-239.

10. Ottensmeyer, M.P., 2001. “Minimally invasive instrument for in vivo measurement of solid organ mechanical impedance”. Ph.D. Thesis, Dept. of Mechanical Engineering, MIT.

11. Gefen, A., Margulies, S.S., 2004. “Are in vivo and in situ brain tissues mechanically similar?”. Journal of Biomechanics, Vol. 37, pp. 1339-1352.

12. Fung, Y.C., 1993. Biomechanics: Mechanical properties of living tissues. 2nd ed. New York, Springer-Verlag.

Figures:

A. Initializations

A.I. Given :

Δt

A.II. Given, for $j = 1, \ldots, N$:

γ_j *and* τ_j

A.III. Given, for $n = 0, \ldots, T_{end}$:

F_{ext}^{n}

A.IV. Zero, for $e = 1, \ldots, N_e$ *and* $j = 1, \ldots, N$:

${}_eh_j^0 \leftarrow 0$

B. Pre - calculations

B.I. Form, for $j = 1, \ldots, N$:

$$A_j = \frac{1 - e^{-\frac{\Delta t}{\tau_j}}}{\frac{\Delta t}{\tau_j}}$$

B.II. Form, for $e = 1, \ldots, N_e$:

$${}_eK_T = {}_eB^T C_{elastic\ e} B_e V \left(1 + \sum_{j=1}^{N} \gamma_j A_j \right)$$

$${}_eK_{hist} = {}_eB^T C_{elastic\ e} B_e V \sum_{j=1}^{N} \gamma_j A_j$$

B.III. Assemble :

$$K_T = \mathrm{A}_{e=1}^{Ne}({}_eK_T)$$

B.IV. Take inverse :

$$K_T^{-1} = I(K_T)$$

B.V. Solve :

$$U^0 = K_T^{-1} F_{ext}^0$$

B.VI. Disassemble, for $e = 1, \ldots, N_e$:

$${}_eU^0 = \mathrm{A}^{-1}(U^0)$$

C. Time - step loop calculations

$n = 0, \ldots, T_{end} - 1$

****

C.I. Calculate, for $e = 1, \ldots, N_e$:

$${}_eH^{n+1} = {}_eV\ {}_eB^T \sum_{j=1}^{N} e^{-\frac{\Delta t}{\tau_j}}\ {}_eh_j^{\,n}$$

$${}_eF_{hist}^{n+1} = {}_eH^{n+1} - {}_eK_{hist}\ {}_eU^n$$

C.II. Assemble :

$$F_{hist}^{n+1} = \mathrm{A}_{e=1}^{Ne}({}_eF_{hist}^{n+1})$$

C.III. Solve :

$$U^{n+1} = K_T^{-1}\left[F_{ext}^{n+1} - F_{hist}^{n+1}\right]$$

C.IV. Disassemble, for $e = 1, \ldots, N_e$:

$${}_eU^{n+1} = \mathrm{A}^{-1}(U^{n+1})$$

C.V. Calculate, for $e = 1, \ldots, N_e$ *and* $j = 1, \ldots, N$:

$${}_eh_j^{\,n+1} = e^{-\frac{\Delta t}{\tau_j}}\ {}_eh_j^{\,n} + \gamma_j A_j C_{elastic\ e} B\left({}_eU^{n+1} - {}_eU^n\right)$$

****

Next n

Figure 1.

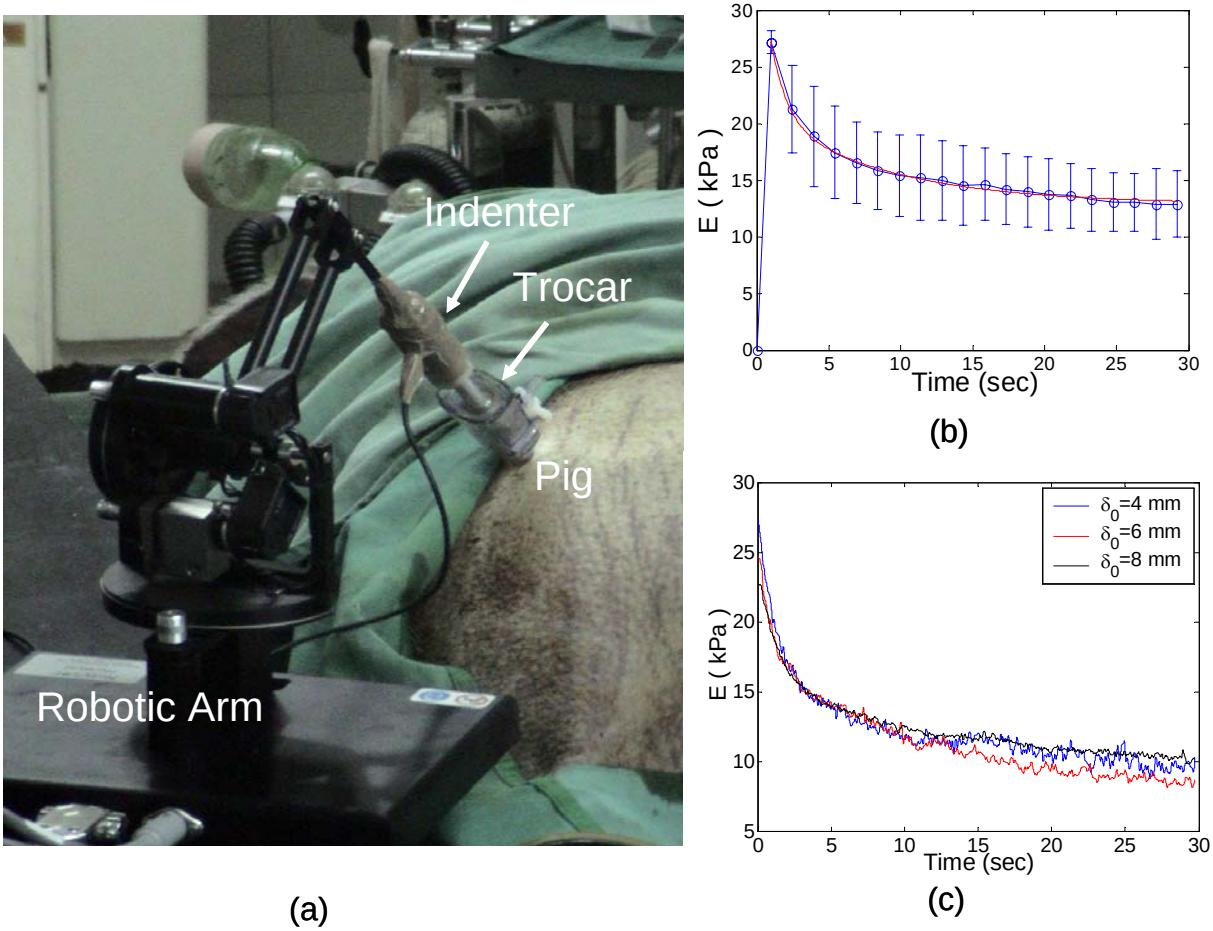
Indenter
Trocar
Pig
Robotic Arm
(a)
E (kPa)
Time (sec)
(b)
δ0=4 mm
δ0=6 mm
δ0=8 mm
E (kPa)
Time (sec)
(c)

Figure 2.

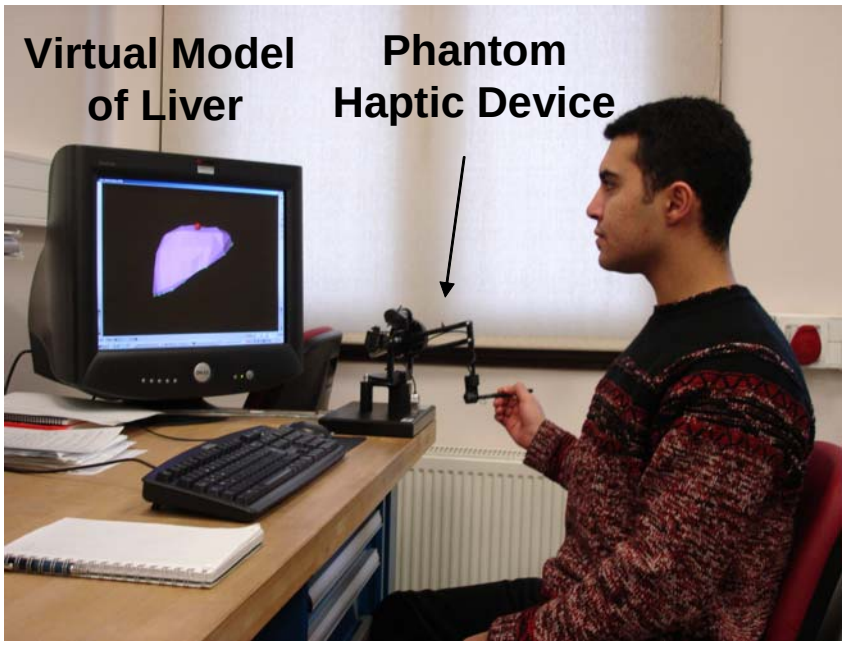
Virtual Model
of Liver
Phantom
Haptic Device

(a)

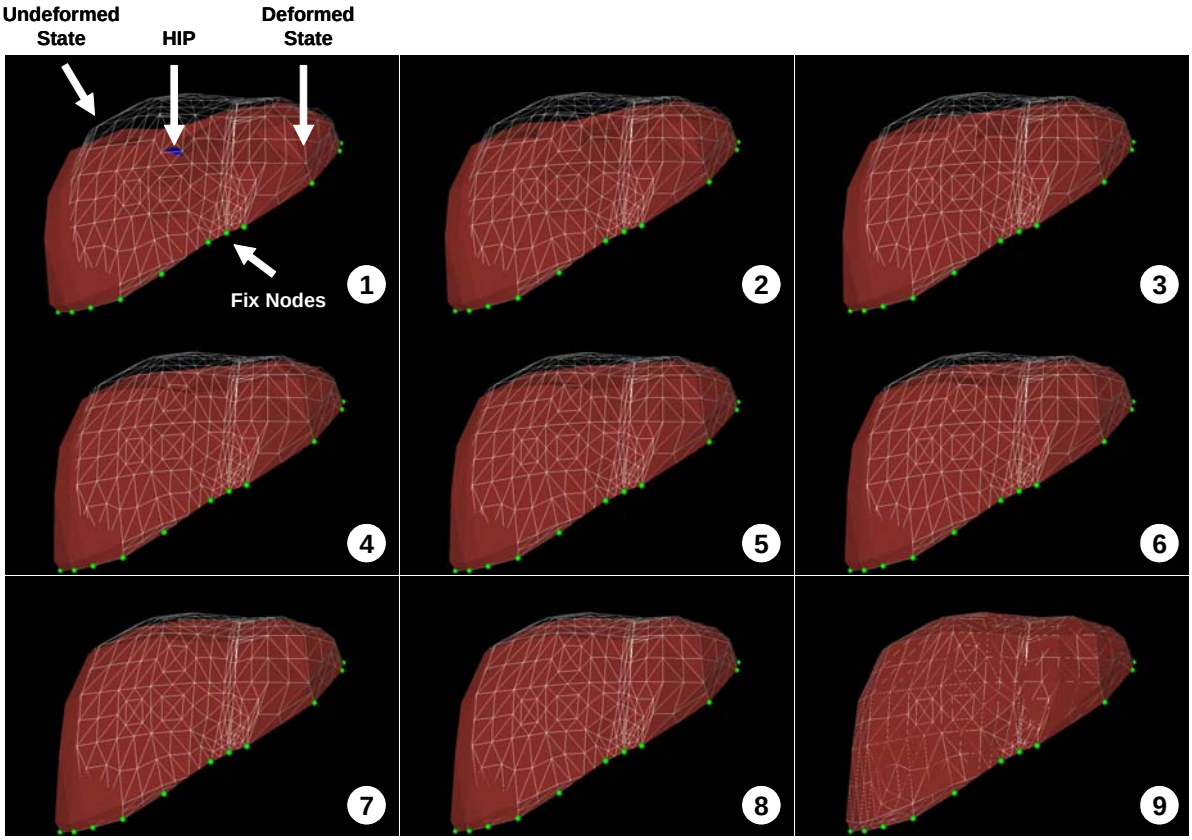
Undeformed
State
HIP
Deformed
State
Fix Nodes
1
2
3
4
5
6
7
8
9

(b)

Figure 3.

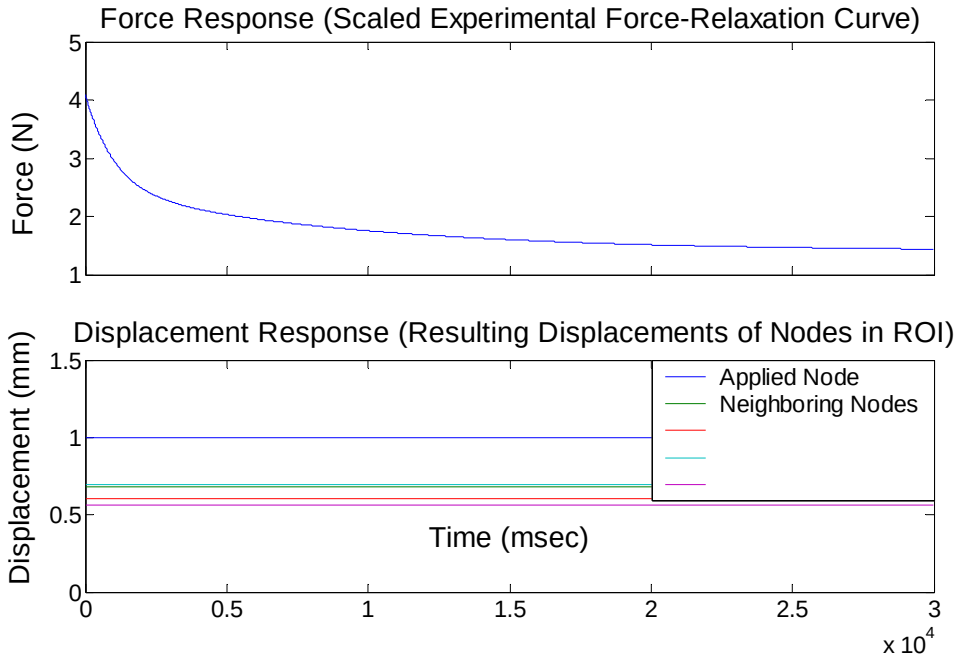

Figure 4a.

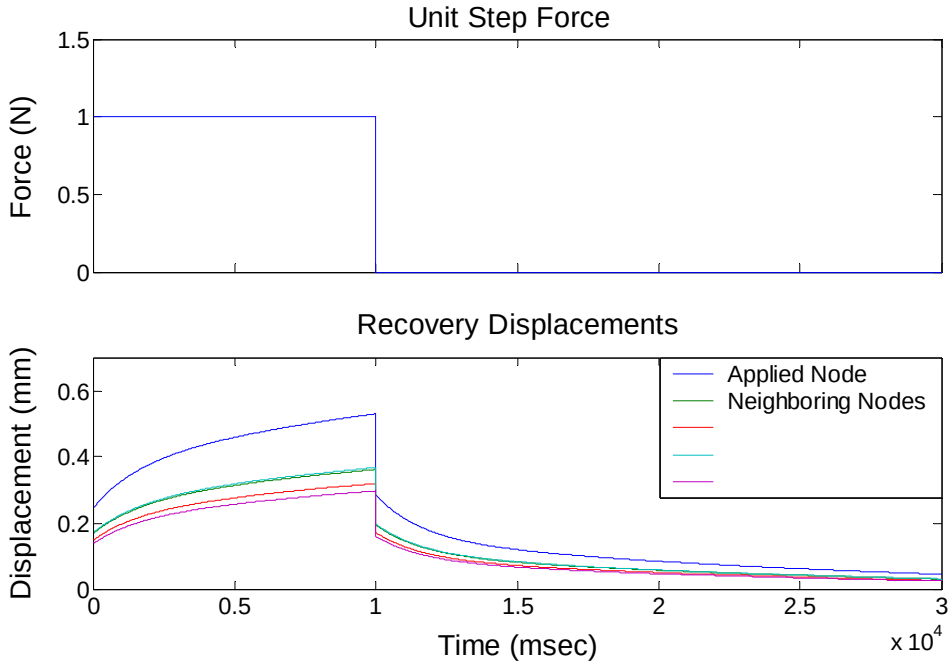

Figure 4b.

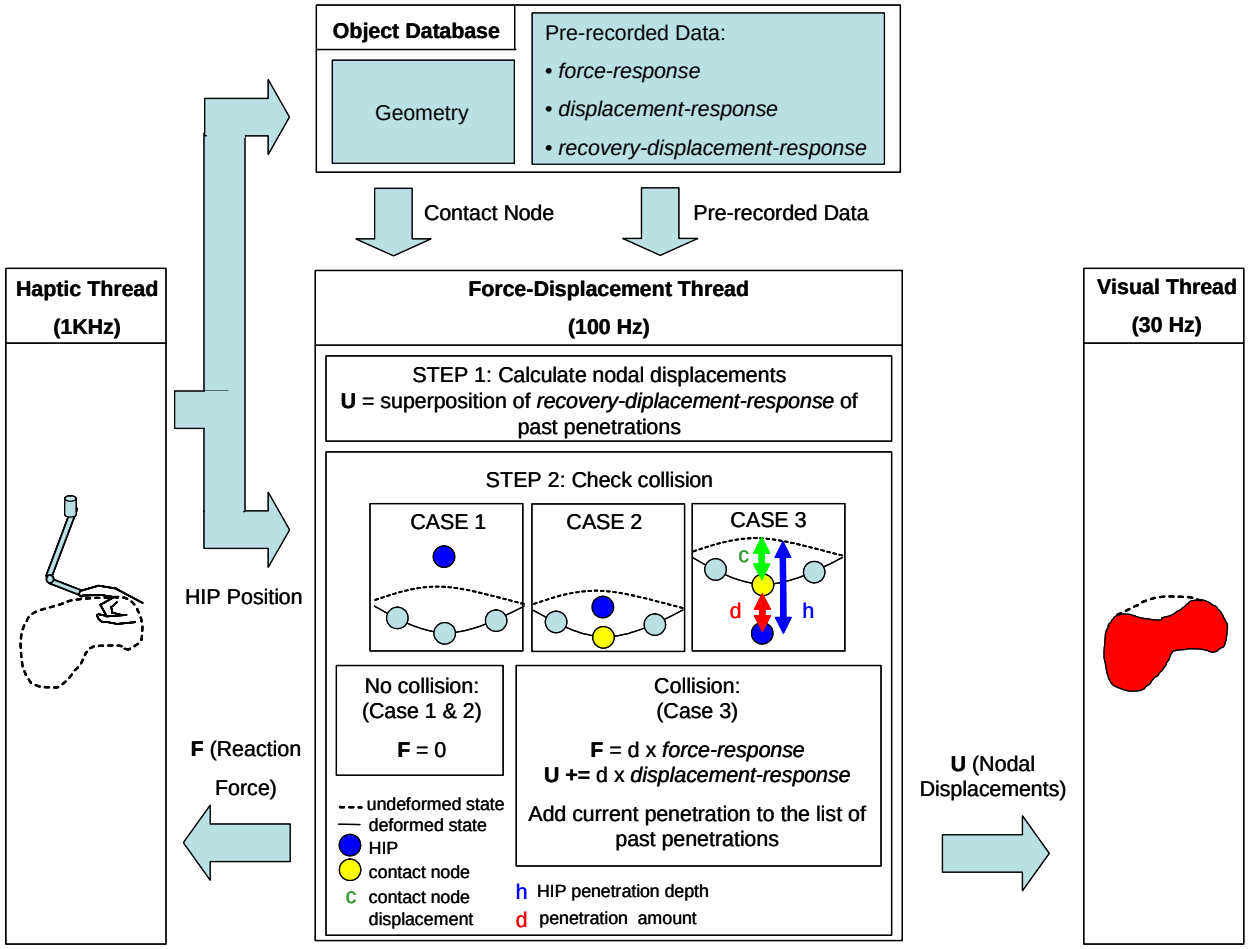
Object Database
Geometry
Pre-recorded Data:
• force-response
• displacement-response
• recovery-displacement-response
Contact Node
Pre-recorded Data
Haptic Thread
(1KHz)
Force-Displacement Thread
(100 Hz)
Visual Thread
(30 Hz)
STEP 1: Calculate nodal displacements
U = superposition of recovery-diplacement-response of past penetrations
STEP 2: Check collision
CASE 1
CASE 2
CASE 3
c
d
h
HIP Position
F (Reaction Force)
No collision:
(Case 1 & 2)
F = 0
Collision:
(Case 3)
F = d x force-response
U += d x displacement-response
Add current penetration to the list of past penetrations
U (Nodal Displacements)
undeformed state
deformed state
HIP
contact node
c contact node displacement
h HIP penetration depth
d penetration amount

Figure 5.

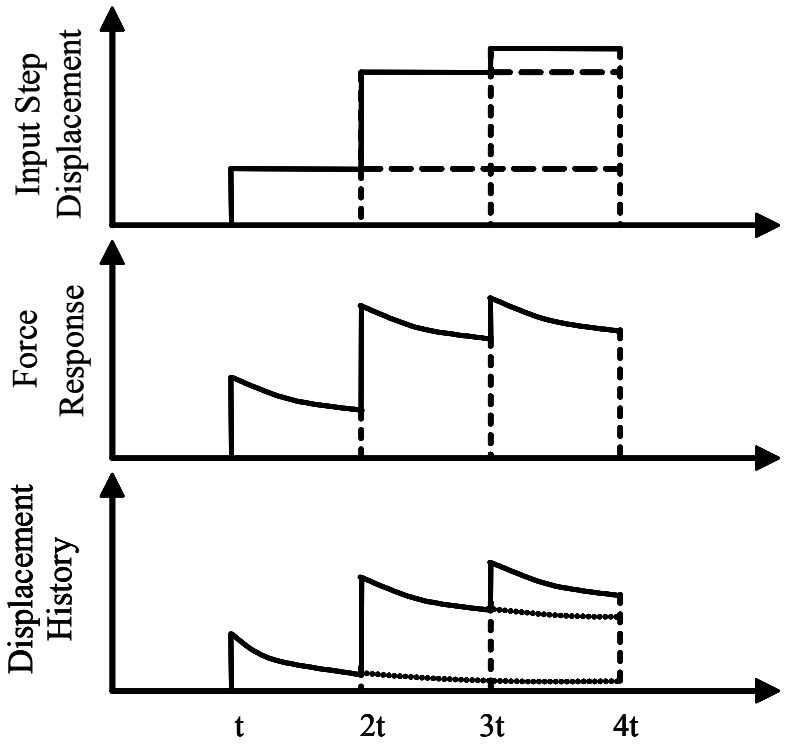
Input Step Displacement
Force Response
Displacement History
t
2t
3t
4t

Figure 6.

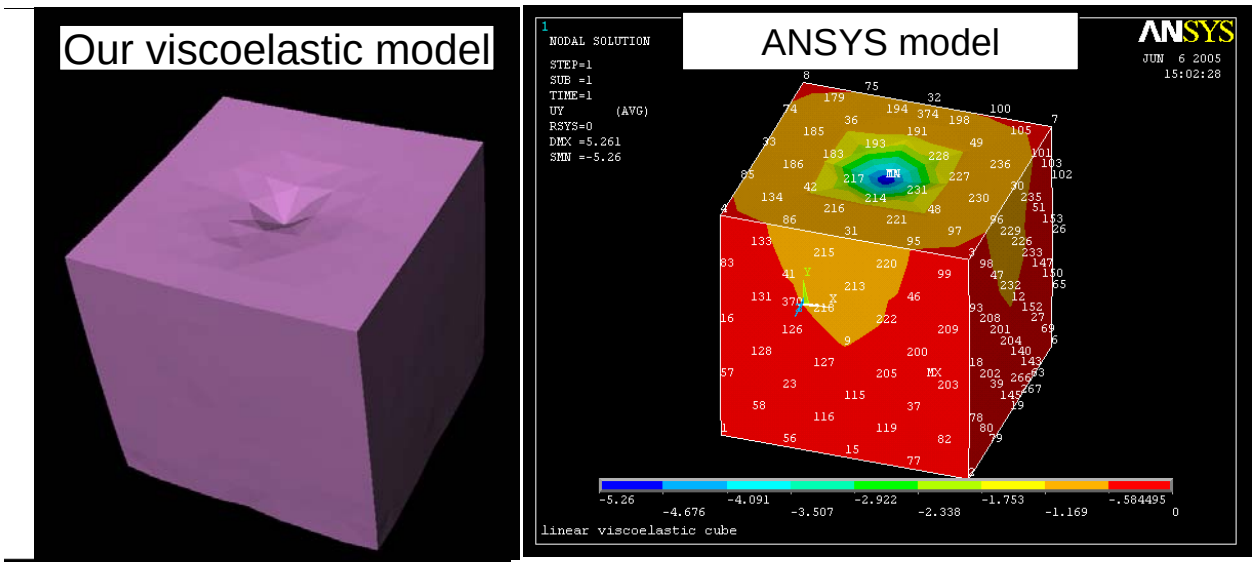
Our viscoelastic model
ANSYS model
NODAL SOLUTION
STEP=1
SUB =1
TIME=1
UY (AVG)
RSYS=0
DMX =5.261
SMN =-5.26
ANSYS
JUN 6 2005
15:02:28
-5.26
-4.676
-4.091
-3.507
-2.922
-2.338
-1.753
-1.169
-.584495
0
linear viscoelastic cube

(a)

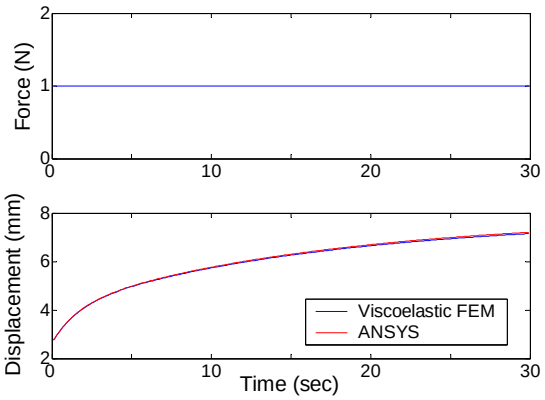
Force (N)
Displacement (mm)
Time (sec)
Viscoelastic FEM
ANSYS

(b)

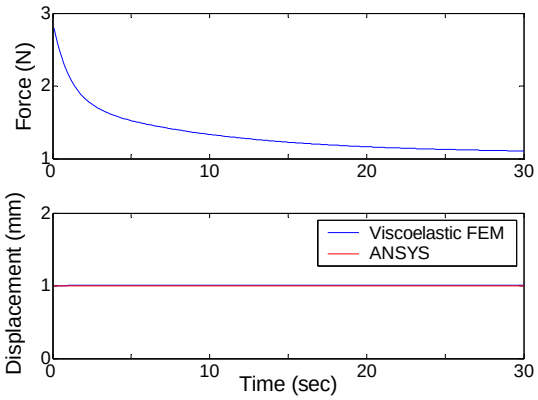
Force (N)
Displacement (mm)
Time (sec)
Viscoelastic FEM
ANSYS

(c)

Figure 7.

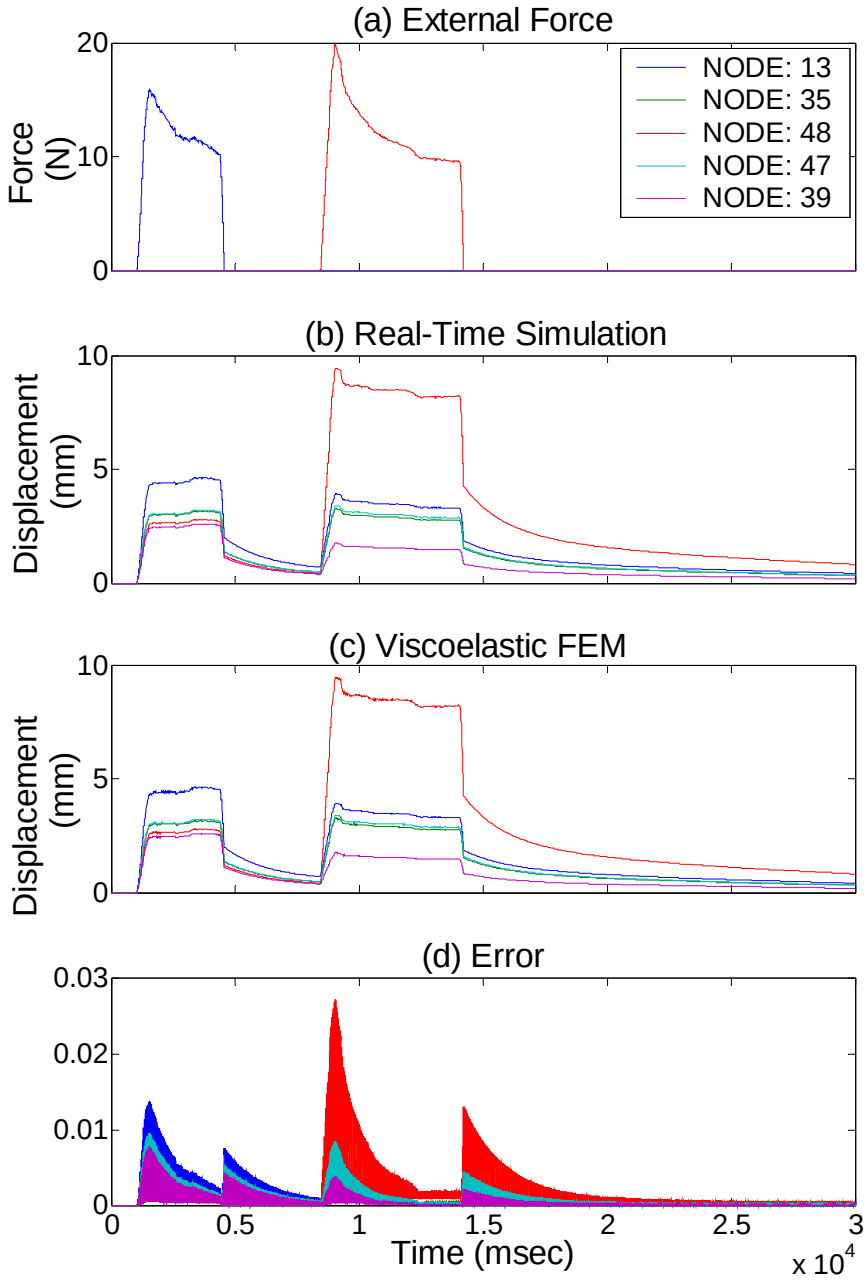
(a) External Force
Force (N)
20
10
0
NODE: 13
NODE: 35
NODE: 48
NODE: 47
NODE: 39
(b) Real-Time Simulation
Displacement (mm)
10
5
0
(c) Viscoelastic FEM
Displacement (mm)
10
5
0
(d) Error
0.03
0.02
0.01
0
0
0.5
1
1.5
2
2.5
3
Time (msec)
x 10^4

Figure 8.

Figure Captions:

Figure 1. The pseudo code for calculating the nodal displacements of our linear viscoelastic finite element model.

Figure 2. a) The components of our robotic system for minimally invasive measurement and characterization of soft tissue behavior. b) The stress relaxation behavior of pig liver for the indentation depth of 4 mm. The red colored curve is the Prony series approximation of the experimental data. c) The stress relaxation function for different depths and loading rates.

Figure 3. a) The components of the simulation system include a computer monitor for displaying visual deformations and a haptic device for displaying reaction forces. b) A series of snapshots showing the viscoelastic relaxation of liver model in response to the force applied briefly to a node on the surface.

Figure 4. a) The Prony series representation of the experimental force relaxation data is scaled and applied to a surface node of a 3D cube such that its displacement response is exactly 1 mm (bottom). b) A unit step force is applied to the same node for 10 sec (top) and then its resultant recovery displacement and that of neighboring nodes are obtained (bottom). The largest displacement is naturally observed at the applied node. Note that the force is applied for 10 sec instead of 10 msec to display the creep response more clearly in the figure.

Figure 5. The flow-chart of our pre-computation approach.

Figure 6. The reaction force displayed to the user (middle) is computed by scaling the *force-response* of the *contact-node* with magnitude of the applied step displacement (top). Recovery effects of past penetrations are scaled by the magnitude of the reaction force and superimposed to each other to compute the displacement history of the *contact-node* (bottom).

Figure 7. a) The first test: we applied 2.0 N to the center node on the top surface of a 3D cube. The displacement response calculated using our viscoelastic finite element model and the one obtained using ANSYS show a perfect agreement up to the second digit after the decimal point (5.26 mm). b) The second test: the cube was compressed by applying unit step force to the nodes on the top surface (top). The displacement response of Node 13 calculated using our viscoelastic FEM and the response obtained using ANSYS shows a perfect agreement (bottom). c) The third test: the cube was compressed by applying unit step displacement to the nodes on the top surface in ANSYS (bottom). The force response data of Node 13 was recorded and then supplied to our viscoelastic FEM as an input to reconstruct the step displacement profile (bottom) which shows a perfect agreement with the step displacement profile given to ANSYS.

Figure 8. To validate the pre-computation approach, external forces were applied to the nodes 13 and 48 of the cube using the haptic probe during the real-time simulations (a). The

displacement response obtained by the superposition approach (b) and the one obtained directly from the viscoelastic FEM (c) are compared to quantify the modeling error (d).